High-Order Sliding-Mode Controllers of an Electropneumatic Actuator: Application to an Aeronautic Benchmark — Source link ↗

Alexis Girin, Franck Plestan, Xavier Brun, Alain Glumineau

Institutions: École centrale de Nantes, Institut national des sciences Appliquées de Lyon

Related papers:

- A study on tracking position control of an electropneumatic system using backstepping design

- Higher order sliding mode control based on optimal approach of an electropneumatic actuator

- Sliding order and sliding accuracy in sliding mode control

- Systematic control of an electropneumatic system: integrator backstepping and sliding mode control

- Sliding mode control with gain adaptation—Application to an electropneumatic actuator

High-Order Sliding-Mode Controllers of an Electropneumatic Actuator: Application to an Aeronautic Benchmark

Alexis Girin, Franck Plestan, Xavier Brun, Alain Glumineau

High order sliding mode controllers of an electropneumatic actuator : application to an aeronautic benchmark

A. Girin[+], F. Plestan[+], X. Brun[*], and A. Glumineau[+]

[+] IRCCyN, UMR CNRS 6597, Ecole Centrale de Nantes, Nantes, France,
{Alexis.Girin,Franck.Plestan,Alain.Glumineau}@irccyn.ec-nantes.fr

[*] Laboratoire AMPERE,UMR CNRS 5005, INSA Lyon, Villeurbanne, France, Xavier.Brun@insa-lyon.fr

Abstract

This paper presents the control of an electropneumatic system used for moving steering mechanism. This aeronautic application needs a high-precision position control and high bandwidth. The structure of the experimental setup and the benchmark on which controllers are evaluated have been designed in order to precisely check the use of such actuator in aeronautics. Two kinds of controllers are designed: a linear one based on gain scheduling feedback, and two high order sliding mode controllers ensuring finite time convergence, high accuracy and robustness. Experimental results display feasibility and high performance of each controller and a comparison study is done.

Keywords. Robust control, high order sliding mode, electropneumatic system.

Nomenclature

y, v, a	position, velocity and acceleration $[m][m/s][m/s^2]$	y_d, v_d, a_d, j_d	desired position, velocity, acceleration and jerk $[m][m/s][m/s^2][m/s^3]$
p_X	pressure in chamber X $[Pa]$	u_P, u_N	servodistributors voltages $[V]$
k	polytropic constant	t_F	fixed time convergence $[s]$
V_X	chamber X volume $[m^3]$	b_v	viscous friction coefficient $[N/m/s]$
F_f	dry friction force $[N]$	M	total moving load mass $[kg]$
T	chambers temperature $[K]$	r_g	perfect gas constant $[J/kg/K]$
S	piston area $[m^2]$	q_m	mass flow rate provided from the servo-distributor $[kg/s]$
$q_{mX_{in}}/q_{mX_{out}}$	mass flow rate brought inside/outside of a chamber $[kg/s]$		

1 Introduction

The present work is motivated by an aeronautic application: the objective consists in evaluating, under a specific benchmark, the performance of a pneumatic actuator when controlling the position of a steering mechanism (Figure 1). As a matter of fact, the use of pneumatic actuators is a solution for high accuracy positioning problem due to their advantages (law maintenance cost, lightweight and good force/weight ratio) in spite of their traditional drawbacks (friction, variation of the actuators dynamics with respect to load and piston position along the cylinder stroke, nonlinearities, ...). One of the advantages of pneumatic energy lies in the fact that, versus electrical energy and in the considered aeronautic context, this kind of energy is still avalaible in aerial vehicles fitted with a turbocharge: as a matter of fact, in a such system, it is possible to recover the unused gas either for control of rudders actuators, either for its storage in an accumalator. Therefore, it yields in an overall energy consumption reduction leading to an overall weight reduction of the system and then a larger duration of the mission (aerial autonomous vehicles or satellites, for example) or the system range (rockets or missiles, for example).

For this specific application, a new experimental setup has been designed that is quite different to previous ones used
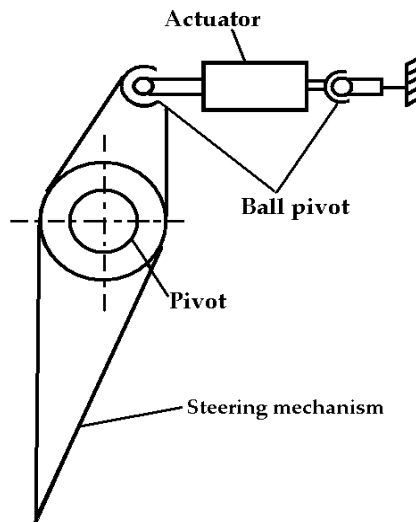
Figure 1: Scheme of a steering mechanism and its actuator.

by the authors [5, 22] because of actuator dynamics (faster), reference trajectories (higher frequency), presence of external disturbance force (springs), actuator dimension (smaller size). Then, through the design of an adequate benchmark, the goal is to evaluate the performance of pneumatic actuator controller by taking into account the aeronautic context: the actuator has to be slight and able to develop sufficient forces with high accuracy/dynamic performances. The development of high-performance linear/nonlinear controllers [30, 16, 35, 12, 19, 5, 8, 9, 20, 29, 40, 41, 11] has shown the positionning feasibility for a pneumatic actuator. However, due to uncertainties, robust controllers are necessary to ensure positioning with high precision. In this way, sliding mode controllers are used for electropneumatic actuators [3, 31, 45, 42]. However, since the sampling frequency of the controller is limited, chattering phenomena appears.

Higher order sliding mode control [25, 1, 26, 21, 22, 32, 33] is a recent approach which allows to remove the standard sliding mode restrictions, while preserving the main sliding-mode features and improving its accuracy. In [25, 1], results only concern second order sliding mode control. In [26], a general approach (for all sliding mode order) is proposed, but the convergence time is only bounded, not exactly known in advance, and the convergence condition is not constructive. The controller proposed in [21, 32] combines standard sliding mode control with linear quadratic one over a finite time interval with a fixed final state. The algorithm needs the relative degree of the system with respect to the sliding variable and the bounds of uncertainties. The upper bound of the convergence time is known and can be adjusted in advance, the condition on the gain implies that its tuning is constructive, and the structure of the controller is well-adapted to practical implementations (pneumatic actuators control in [22]). However, two drawbacks appear with this approach. It ensures only a *practical* sliding mode establishment (only convergence in finite time to an arbitrarily small vicinity of the origin is ensured), and the reaching time is bounded but cannot be fixed *exactly* and in advance. In [23, 33], these two drawbacks (sliding variable and its time derivatives are *exactly* at 0 in finite time) are erased, and the convergence time is imposed by keeping all the features of the previous approach (general order of sliding mode, finite time convergence, constructive approach). Results in [23] are based on integral sliding mode concept and need an auxiliary dynamic system in order to compute the switching variable. Note also that high order sliding mode control based on integral sliding mode is also proposed in [27]. In [33], the approach, which is selected for this current work, consists in computing adequate reference trajectories which ensure that the higher order sliding mode is established at the desired time, in spite of uncertainties.

In Section 2, a benchmark is given and the experimental setup is described. Section 3 displays nonlinear and linear models of the system and the associated assumptions. Section 4 presents a linear feedback control with experimental
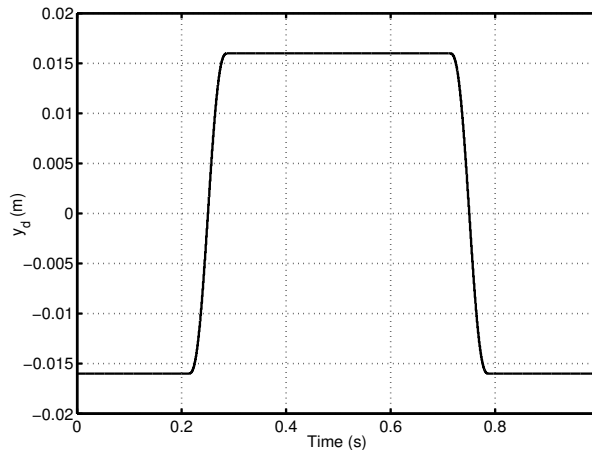
Figure 2: **Low altitude flight:** Actuator desired position (*m*) versus time (*s*).

results in order to establish performance comparisons with other controllers. Section 5 displays the high order sliding mode controller in single input-single output (SISO) context (only actuator position control) with experimental results. In Section 6, a multi input-multi output (MIMO) high order sliding mode controller (actuator position and chamber pressure control) is designed and experimental results are given. For this system, the main advantage of multivariable control is no zero dynamics (in SISO case, it is a very difficult task to formally prove the zero dynamics stability [5]). Furthermore, as one of the pressure is controlled, it is possible to act on the actuator accuracy and rigidity in case of perturbation. This latter feature is a key point for the current application, because the steering mechanism position has to be as accurate and rigid as possible with respect to external perturbation.

2   Benchmark and experimental setup

Most of aeronautic applications use electric or hydraulic actuators for steering mechanisms. Currently pneumatic actuators are rarely used in such applications because of their weak (static and dynamics) performances when controlled by standard components and classical controllers. The new challenge exposed in this paper consists in improving their performances by application of advanced control strategies to obtain the high performances required in aeronautics. Thus, by taking into account the aeronautic context, a specific benchmark is designed for evaluation of controller performances.

2.1   Benchmark

In the sequel, typical dynamic and static desired performances of aeronautic steering mechanims *in a reduced scale* are described through a specific benchmark. Several desired actuator position trajectories are described, each trajectory being typical of a flight phase (high, medium or law altitude) (see Figure 2 for low altitude trajectory)

- High altitude: ± 4 *mm* actuator position trajectory with 1 *Hz* frequency and ± 300 *N* maximum load force,

- Medium altitude: ± 12 *mm* actuator trajectory with 1 *Hz* frequency and ± 900 *N* maximum load force,

- Low altitude: ± 16 *mm* actuator trajectory with 1 *Hz* frequency and ± 1200 *N* maximum load force .

Note that desired position trajectories are such that velocity, acceleration and jerk are continuous functions. In order to evaluate dynamics performances of closed-loop system, a Bode diagram is defined (Figure 3), by supposing that the desired position trajectory reads as a sinusoidal signal with an amplitude equal to 16 *mm*. For each desired trajectory displayed in Figure 2, the closed-loop system has to fulfill the following performances
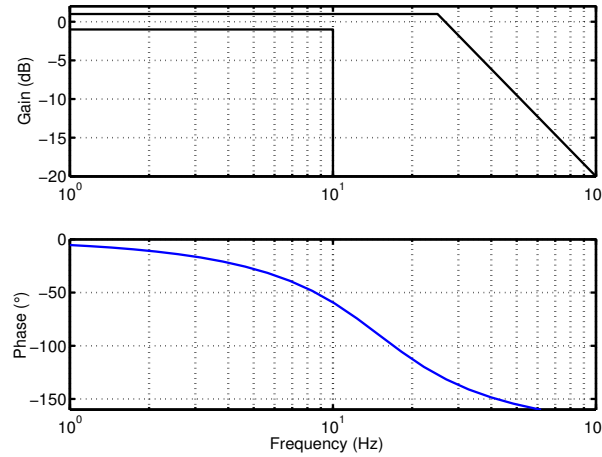
Figure 3: Bode template. **Top** - Gain (*dB*) versus frequency (*Hz*). **Bottom.** Phase (*deg*) versus frequency (*Hz*).

- The static error ε_p is such that $\varepsilon_p \leq 0.2$ *mm*,

- The rise time t_r maximum value is fixed through the minimum desired velocity 0.4 *m/s* for 32 *mm* displacement, which gives $t_r \leq 0.08$ *s*

- The overshoot is lower than 4.6 %.

On aeronautic applications, space and weight are crucial for performances and technical solution feasibility. For this reason, in the case of pneumatic actuator, the total fluid consummation used during a typical flying sequence (succession of low, medium and high altitudes) is evaluated: of course the objective is to bring the smaller fluid tank.

2.2 Electropneumatic system

The electropneumatic system under interest is a double acting actuator controlled by two servodistributors (see Figure 4) and composed by two chambers denoted P (as positive) and N (as negative). Piston diameter is 63 *mm* and rod diameter is 16 *mm*. With a 7 *bar* source pressure, the actuator maximum force is 1750 *N*. The air mass flow rates q_m entering in the chambers are modulated by two three-way servodistributors Servotronic (Asco-Joucomatic) controlled by a micro-controller. The pneumatic jack horizontally moves a load carriage of mass M. This carriage is coupled to 4 springs (which restrain the displacement of the carriage and restore the initial position in the middle of the total stroke equal to 50 mm - see Figure 4) for a total of 63000 N/m rate. Additional dry friction is controlled by two skates, with a maximum value equal to 40 *N*. As the maximal displacement of carriage is 16 *mm*, the maximal disturbance spring force F_s equals 1200 *N*. The electropneumatic plant model is obtained from three physical laws: the mass flow rate through a restriction, the pressure behavior in a variable chamber volume and the fundamental mechanical equation. The experimental setup is simulated with a fluid power systems dedicated software AMESim (Imagine SA), and the control law is developed with Matlab/Simulink (Mathworks). These software choices imply a cosimulation program [7] and the development of two models

- the first one takes into account physical phenomena as temperature variations, practical values of mass flow rate, dynamics of servodistributors. It is developed under AMEsim.

- the second one is simpler than the previous one and is used to design the controller (Simulink). In this paper, experimental results are exclusively presented: only control models are described in the sequel.
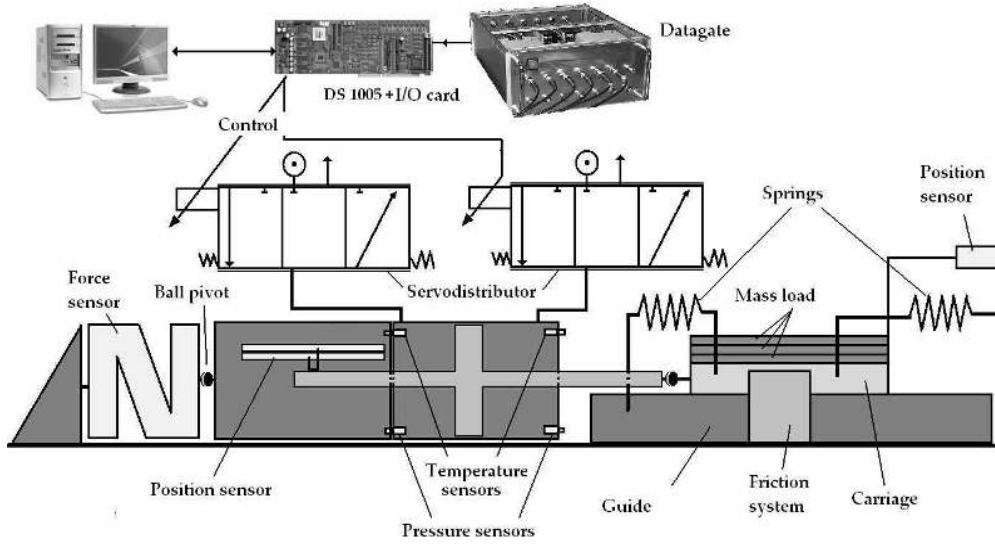
4

Figure 4: Electropneumatic system scheme.

3 Models of the experimental setup

3.1 Nonlinear model

3.1.1 Pressure dynamics

Each chamber of the pneumatic actuator is considered as a variable volume, in which the air mass evolves with time. State the following assumptions

A1. Air is a perfect gas ands its kinetic is inconsequential.

A2. The pressure and the temperature are homogeneous in each chamber.

A3. The mass flow is pseudo-stationary.

A4. Dynamic part of servodistributor is neglected.

A5. The temperature variations in each chamber are inconsequential with respect to the supply temperature T.

A6. The process is polytropic and characterized by coefficient k (with $1 < k < 1.4$) [38].

Then, pressures dynamics read as (with $X = P$ or N)

$$\frac{dp_X}{dt} = -k\frac{p_X}{V_X}\frac{dV_X}{dt} + \frac{kr_gT}{V_X}\left(q_{mX_{in}} - q_{mX_{out}}\right) \tag{1}$$

with $q_{mX_{in}}$ the mass flow rate brought inside the X chamber and $q_{mX_{out}}$ the mass flow rate brought outside the X chamber, V_P and V_N being the volume of chambers P and N defined as $V_P(y) = V_0 + S \cdot y$ and $V_N(y) = V_0 - S \cdot y$ (V_0 being equal to the half of the cylinder volume.

A7. The leakages between the two chambers and between servodistribuor and jack are negligible.

By defining $q_m(u_X, p_X) := q_{mX_{in}} - q_{mX_{out}}$, one gets

$$
\begin{aligned}
\frac{\mathrm{d}p_P}{\mathrm{d}t} &= -k\frac{p_P}{V_P(y)}\frac{\mathrm{d}V_P(y)}{\mathrm{d}t} + \frac{kr_gT}{V_P}q_m(u_P, p_P) \\
\frac{\mathrm{d}p_N}{\mathrm{d}t} &= -k\frac{p_N}{V_N(y)}\frac{\mathrm{d}V_N(y)}{\mathrm{d}t} + \frac{kr_gT}{V_N}q_m(u_N, p_N)
\end{aligned}
\tag{2}
$$

A8. Mass flow rate has been identified by the following function

$$
q_m(u_X, p_X) = \varphi_X(p_X) + \psi_X(p_X, \mathrm{sign}(u_X))u_X
$$

with φ_X and ψ_X defined as 5th-order polynomials with respect to p_X [2].

A9. All dry frictions forces are neglected.

A10. There is no control signal saturation.

3.1.2 Mechanical model

The second Newton law gives

$$
\begin{aligned}
\frac{\mathrm{d}v}{\mathrm{d}t} &= \frac{1}{M}[S(p_P - p_N) - b_v v - F_s] \\
\frac{\mathrm{d}y}{\mathrm{d}t} &= v
\end{aligned}
\tag{3}
$$

with F_s the springs force.

A11. Springs force F_s is unknown and viewed as a bounded external perturbation[1], *i.e.* $|F_s| < \Delta F$.

3.1.3 MIMO nonlinear model

Knowing that uncertainties taken into account in the control design concern polytropic constant k (such that $k = 1.2 + \Delta k$ with $|\Delta k| \le 0.2$), mass flow q_m, temperature T, mass M, viscous friction coefficient b_v, and that there is bounded external perturbation F_s, the experimental setup nonlinear model reads as

$$
\begin{aligned}
\dot{p}_P &= \frac{(1.2 + \Delta k)r_g(T + \Delta T)}{V_P(y)}[\varphi_P + \Delta\varphi - \frac{S}{r(T + \Delta T)}p_P v] + \frac{(1.2 + \Delta k)r_g(T + \Delta T)}{V_P(y)}(\psi_P + \Delta\psi)u_P \\
\dot{p}_N &= \frac{(1.2 + \Delta k)r_g(T + \Delta T)}{V_N(y)}[\varphi_N + \Delta\varphi + \frac{S}{r(T + \Delta T)}p_N v] + \frac{(1.2 + \Delta k)r_g(T + \Delta T)}{V_N(y)}(\psi_N + \Delta\psi)u_N \\
\dot{v} &= (M^{-1} + \delta M)[Sp_P - Sp_N - (b_v + \Delta b_v)v - \Delta F] \\
\dot{y} &= v
\end{aligned}
\tag{4}
$$

with $|\Delta T| < T_M$, $|\Delta\varphi| < \varphi_M$, $|\Delta\psi| < \psi_M$, $|\delta M| < M_M$, $|\Delta b_v| < b_{vM}$ and $|F_s| < \Delta F$; T_M, φ_M, ψ_M, M_M, b_{vM} and ΔF being all bounded real values. Position, pressures and control are limited by physical domain as $-18\ mm \le y \le +18\ mm$, $1\ bar \le p_X \le 7\ bar$ and $-10\ V \le u_X \le 10\ V$.

---

[1]This hypothesis is taken due to the context: in fact, on the experimental setup, springs are modeled in a very simple way, the air on the steering mechanism during the flight. Of course, in this latter real situation, this external force is not easy to evaluate. Then, the controllers do not use this value.

3.1.4 SISO nonlinear model

As the experimental set-up is equiped by two servodistributors, a such structure allows to define only one control objective (for example, actuator position) [4] by fulfilling the following assumption

A11. In SISO case, only the actuator position is controlled: the single control u_S reads as $u_S = u_P = -u_N$.

It yields that the experimental setup nonlinear model in a SISO context reads as

$$
\begin{aligned}
\dot{p}_P &= \frac{(1.2+\Delta k)r_g(T+\Delta T)}{V_P(y)}[\phi_P + \Delta\phi - \frac{S}{r(T+\Delta T)}p_P v] + \frac{(1.2+\Delta k)r_g(T+\Delta T)}{V_P(y)}(\psi_P(p_P, sign(u_S)) + \Delta\psi)u_S \\
\dot{p}_N &= \frac{(1.2+\Delta k)r_g(T+\Delta T)}{V_N(y)}[\phi_N + \Delta\phi + \frac{S}{r(T+\Delta T)}p_N v] - \frac{(1.2+\Delta k)r_g(T+\Delta T)}{V_N(y)}(\psi_N(p_N, sign(-u_S)) + \Delta\psi)u_S \\
\dot{v} &= (M^{-1}+\delta M)[Sp_P - Sp_N - (b_v + \Delta b_v)v - \Delta F] \\
\dot{y} &= v
\end{aligned}
$$

$$(5)$$

with $|\Delta T| < T_M$, $|\Delta\phi| < \phi_M$, $|\Delta\psi| < \psi_M$, $|\delta M| < M_M$, $|\Delta b_v| < b_{vM}$ and $|F_s| < \Delta F$ as previously. Position, pressures and control are limited by physical domain as $-18\ mm \le y \le +18\ mm$, $1\ bar \le p_X \le 7\ bar$ and $-10\ V \le u_X \le 10\ V$.

3.2 SISO linear model

The equilibrium set reads as

$$\dot{x} = f(x^e, u_S^e) = 0.$$

By supposing that there is no uncertainty on (4), it yields $y = y^e$, $v = v^e = 0$, $S(p_P^e - p_N^e) - b_v v^e = 0$, $q_{mP}^e = q_{mN}^e = 0$. Note that, at the equilibrium set, for all position y^e, the velocity v is null, the pressure in both chambers p_P and p_N are the same. In fact, the springs tends to bring back the position to zero. For all position except zero, the real equilibrium set is defined by $S(p_P^e - p_N^e) - F_s = 0$. Note that for all control law synthesis, the springs force (viewed as an external perturbation) is considered as unknown. From [4], the tangent linearized model reads as

$$
\begin{bmatrix} \dot{p}_P \\ \dot{p}_N \\ \dot{v} \\ \dot{y} \end{bmatrix} =
\begin{bmatrix}
-\frac{1}{\tau_P^e} & 0 & -\frac{kp_P^e S}{V_P(y^e)} & 0 \\
0 & -\frac{1}{\tau_N^e} & \frac{kp_N^e S}{V_N(y^e)} & 0 \\
\frac{S}{M} & -\frac{S}{M} & -\frac{b_v}{M} & 0 \\
0 & 0 & 1 & 0
\end{bmatrix}
\cdot
\begin{bmatrix} p_P \\ p_N \\ v \\ y \end{bmatrix}
+
\begin{bmatrix}
\frac{kr_g T}{V_P(y^e)}G_{uP}^e \\
-\frac{kr_g T}{V_N(y^e)}G_{uN}^e \\
0 \\
0
\end{bmatrix}
u_S
$$

$$(6)$$

with τ_P^e and τ_N^e defined as

$$\tau_P^e = \frac{V_P(y^e)}{kr_g T C_{p_P P^e}} \quad , \quad \tau_N^e = \frac{V_N(y^e)}{kr_g T C_{p_N N^e}}$$

$$(7)$$

and

$$C_{p_P P^e} = -\frac{\partial q_m(u_S^e, p_P)}{\partial p_P}\bigg|_e, \quad G_{u_P^e} = \frac{\partial q_m(u_S, p_P^e)}{\partial u_S}\bigg|_e \quad C_{p_N N^e} = -\frac{\partial q_m(-u_S^e, p_N)}{\partial p_N}\bigg|_e, \quad G_{u_N^e} = -\frac{\partial q_m(-u_S, p_N^e)}{\partial u_S}\bigg|_e$$

$$(8)$$

In the pneumatic field, conventional position control laws consist in position, velocity and acceleration feedbacks. The use of acceleration feedback instead of pressure or differential pressure can be justified by the fact that acceleration is quickly influenced by an external perturbation force. Moreover, the use of a pressure sensor is a hard task due to the very small size of the dead volume. Only position sensor is used, velocity and acceleration being obtained via a robust differentiator [39]. In order to obtain a third order model with position, velocity and acceleration state variables, a
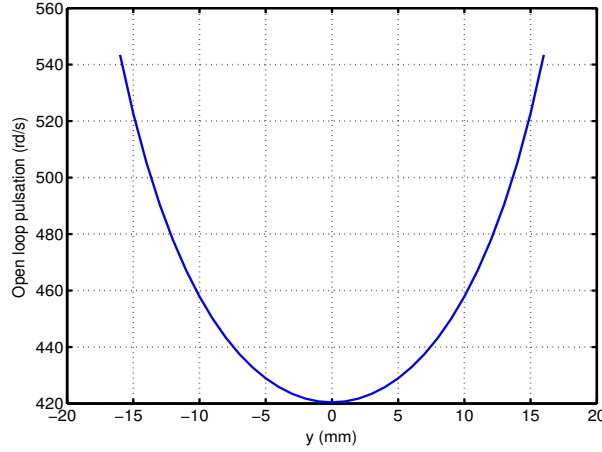
Figure 5: **Linear reduced model.** Open-loop proper frequency ω_{ol} ($rad.s^{-1}$) versus rod position y (mm).

solution consists in replacing each time constant of each chamber by an average time constant τ_m^e (geometric mean) [28]. Then, a reduced SISO linear model is obtained

$$
\begin{bmatrix} \dot{y} \\ \dot{v} \\ \dot{a} \end{bmatrix} = \begin{bmatrix} 0 & 1 & 0 \\ 0 & 0 & 1 \\ 0 & -\omega_{ol}^2 & -2z_{ol}\omega_{ol} \end{bmatrix} \begin{bmatrix} y \\ v \\ a \end{bmatrix} + \begin{bmatrix} 0 \\ 0 \\ b \end{bmatrix} u_S \tag{9}
$$

with

$$
b = \frac{kr_gT}{M}\left[\frac{SG_{u_P^e}}{V_P(y^e)} + \frac{SG_{u_N^e}}{V_N(y^e)}\right] \tag{10}
$$

The damping coefficient denoted z_{ol} reads as

$$
z_{ol} = \frac{1}{2\omega_{ol}}\left[\frac{1}{\tau_m^e} + \frac{b_v}{M}\right] \tag{11}
$$

The open loop proper frequency ω_{ol} equals

$$
\omega_{ol} = \sqrt{\omega_{cyl}^2 + \frac{b_v}{\tau_m^e M}} \tag{12}
$$

with

$$
\omega_{cyl} = \sqrt{\frac{kS}{M}\left(\frac{p_P^e}{V_P(y^e)} + \frac{p_N^e}{V_N(y^e)}\right)} \tag{13}
$$

Remark that all the parameters depend on the piston position as shown by Figure 5; the open loop proper frequency is minimum for the central position.

4   Linear position control

In this section, a SISO linear control based on gain scheduling (GS) and designed from the reduced SISO linear model (9) is presented and experimentally evaluated on the experimental setup. This approach has still been applied on an electropneumatic actuator in [5] and is displayed here only to be compared with more advanced robust nonlinear controllers. The gain scheduling approach is a very classical and widespread nonlinear control technique. The underlying idea is to design at one or more operating points linear time invariant controllers using the associated linearized plant models. The nonlinear control law is then obtained by interpolating (or scheduling) these controllers as a function of the operating point [34, 24, 36, 13].
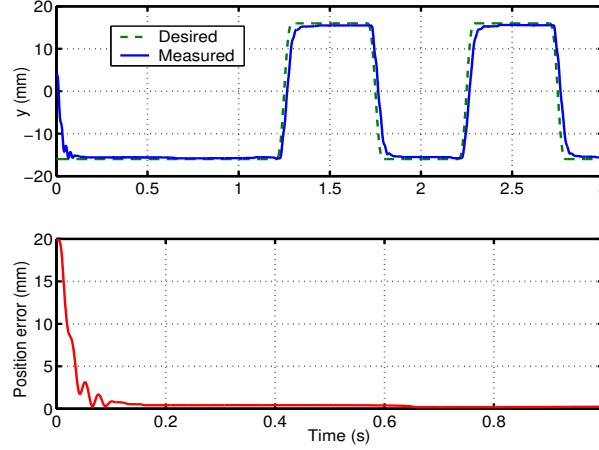
Figure 6: **Nominal case** - **Top.** Desired and current positions (*mm*) versus time (*s*). **Bottom.** Position tracking error (*mm*) versus time (*s*).

4.1 Control design

The control law reads as

$$u_S \quad = \quad K_y(y_d)(y - y_d) + K_v(y_d)v + K_a(y_d)a \tag{14}$$

This controller has been designed from (9) by computing gains K_y, K_v and K_a by Ackerman's approach such that poles placement authorizes 4.6% overshoot [17] as defined in benchmark, Section 2.

The gains are calculated in order to have the maximum of bandwidth compared to actuator variable position. Of course, K_y, K_v and K_a depend on the desired position (gain scheduling method). As detailed in [5], for different positions along the stroke, gains are calculated. Then, each gain is viewed as a second order polynomial with respect to the position, coefficients of this polynomial being obtained from interpolation and approximation with the least square method.

4.2 Application on experimental setup

The control law is implemented on DS1005 Board (dSpace Co.) with a 1 *ms* sample time. Two kinds of experimental tests have been made. The first one, named "Nominal case", consists in moving a mass equal to 0.8*kg* (the control law has been designed with this hypothesis) in presence of springs force disturbance. The second one, named "Robust case", consists in increasing the moving mass to 1.8*kg* (+125%) *without changing the controller gains and always in presence of springs force disturbance*. For a sake of clarity, only results for "low altitude trajectory" which is the most difficult trajectory are displayed in the sequel.

Nominal case. The actuator position (Figure 6) converges to the desired trajectory more than 0.6 *s* with a control saturation at the initial time. The maximum error position in steady state is 0.48*mm* (Figure 7-Bottom) which means that the developed actuator force allows to compensate springs force. During all trajectory tracking, there is no pressure saturation (Figure 7-Top), and control input has wise values (Figure 7-Bottom). Performances have been evaluated on three trajectories, through the static position error. The results are summarized in Table 1. The static position error is minimal when the amplitude trajectory is small. Of course, when the position amplitude increases, springs force also increases. This result shows the limit of gain scheduling control in order to compensate unknown perturbations, and then justifies the interest of the robust nonlinear controllers designed in the sequel.

Altitude	Low ($\pm16mm$)	Medium ($\pm12mm$)	High ($\pm4mm$)
Static position error	0.48	0.38	0.16

Table 1. Static position error (*mm*) with gain scheduling controller.
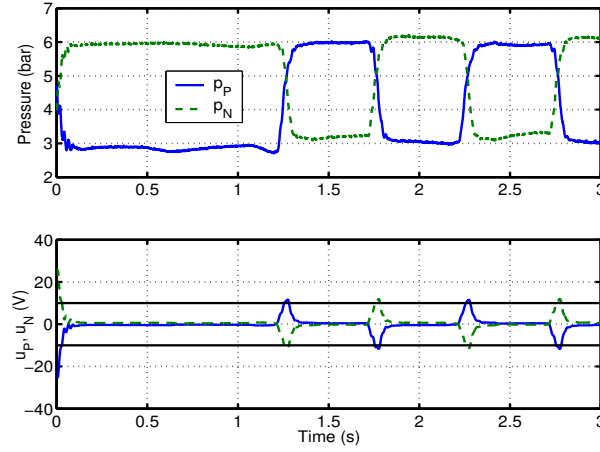
9

Figure 7: **Nominal case** - **Top.** Pressures p_P and p_N (*bar*) versus time (*s*). **Bottom.** Control signals u_P and u_N (*V*), and saturation line (*V*) versus time (*s*).
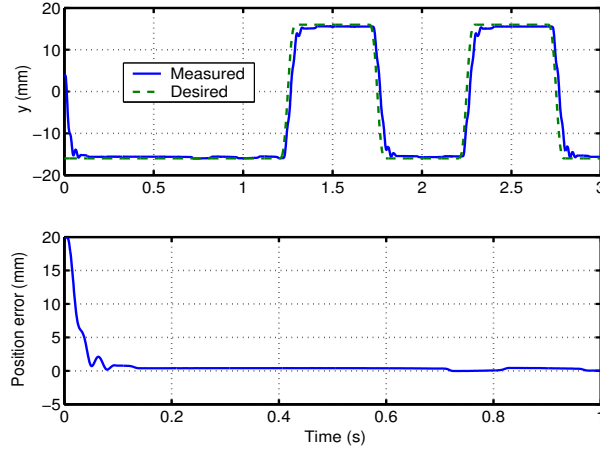

Figure 8: **Robustness evaluation** - **Top.** Desired and current positions (*mm*) versus time (*s*). **Bottom.** Position tracking error (*mm*) versus time (*s*).

Robustness evaluation. The convergence time is 0.72 *s* (Figure 8). The maximum error position in steady state is the same that previously and there is still control saturation at the initial time.

Frequency response. The frequency response (Fig. 9) is evaluated from the 1st harmonic of the position measurement. The gain (resp. the phase) is lower than the gain (resp. the phase) template, thus the bandwidth is lower than the desired one. In fact, the gain is limited by mass flow rate saturation and could be significantly increased by using another servodistributor with highest maximum mass flow rate. On the other hand, the phase can be increased by using an other controller, as seen in the sequel of the paper.

Consumption. The consumption is evaluated over a typical flying sequence (*i.e.* succession of low, medium and high altitude trajectories) and reads as ($X = P$ or N, $q_{mX_{in}}$ being the mass flow rate brought inside the X chamber)

$$C_X = \int_0^{t_{fly}} q_{mX_{in}} \, \mathrm{d}t \tag{15}$$

Unfortunately, the mass flow rate is not measurable in a dynamic context, because it does not exist adequate sensor with sufficient bandwidth. As seen previously, the mass flow rate has been identified in terms of pressures and control
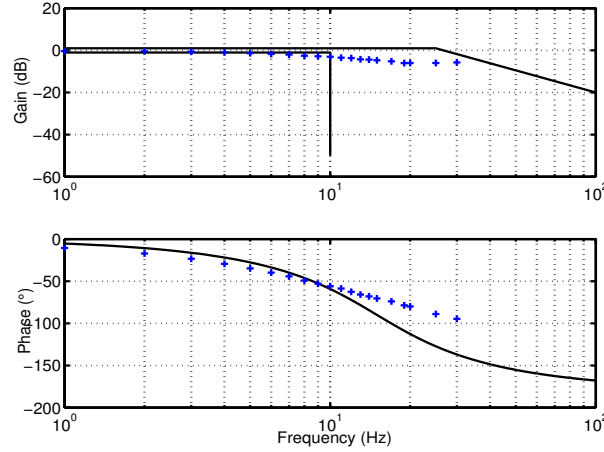
Figure 9: Bode diagram of closed-loop system.

input [37]: then the consumption is computed by simulation [6] from (15) from experimental datas (Table 2).

Consumption C_P	463 g
Consumption C_N	420 g

Table 2. **Gain scheduling controller.** Total consumption in each chamber during a flying sequence.

5 High order sliding mode position controller (SISO)

If a high accuracy position control is the objective, assumptions for the model design imply that a robust control law with respect to uncertainties (frictions, mass flow rate, temperature variations, ...) and perturbations (mass variation, spring force, ...) is required. From [33], a high order sliding mode controller is derived. Its main features are robustness, finite time convergence and high accuracy performances. In the sequel, theorical aspects on this control and its application to the pneumatic system are developed.

5.1 Synthesis of high order sliding mode controller (SM)

Consider an uncertain nonlinear system

$$
\begin{aligned}
\dot{x} &= f(x) + g(x)w \\
z &= h(x)
\end{aligned}
\tag{16}
$$

with $x \in \mathbb{R}^n$ the state variable, $w \in \mathbb{R}$ the input control and $z \in \mathbb{R}$ a measured smooth output function. Let $s(x,t)$ denote the sliding variable defined as $s(x,t) = h(x) - h_d(t)$, $h_d(t)$ being the smooth desired trajectory. $f(x)$ and $g(x)$ are uncertain smooth nonlinear functions. Assume that

H1. The relative degree r [18] of (16) with respect to s is constant and known.

The control objective is to fulfill the constraint $s(x,t) = 0$ in finite time and to keep it exactly by feedback control.

Definition 1 [26] *Consider the nonlinear system (16), closed by some possibly-dynamical discontinuous feedback. Then, provided that[2] s, $\dot{s}$, $\cdots$, $s^{(r-1)}$ are continuous functions, and the set*

$$
\mathbf{S}^r = \{x \mid s(x,t) = \dot{s}(x,t) = \cdots = s^{(r-1)}(x,t) = 0\},
$$

called "r^{th} order sliding set", is non-empty and is locally an integral set in the Filippov sense [14], the motion on $\mathbf{S}^r$ is called "r^{th} order sliding mode" with respect to the sliding variable s.

---

[2]All over this paper, $s(\cdot)^{(k)}$ ($k \in \mathbb{N}$) denotes the kth time derivative of the function $s(\cdot)$. This notation is also applied for every function.

The rth order sliding mode control approach allows the finite time stabilization to zero of the sliding variable s and its $r-1$ first time derivatives by defining a suitable discontinuous control function. The output s satisfies

$$
\begin{aligned}
s^{(r)} &= \bar{\chi}(x) + \Gamma(x)w - h_d^{(r)}(t) \\
&:= \chi(\cdot) + \Gamma(\cdot)w
\end{aligned}
\tag{17}
$$

with[3] $\Gamma := L_g L_f^{r-1} h$, $\bar{\chi} := L_f^r h$ and $\chi := \bar{\chi} - h_d^{(r)}(t)$[33].

H2. The solutions are understood in the Filippov sense [14], and system trajectories are supposed to be infinitely extensible in time for any bounded Lebesgue measurable input.

H3. Functions $\chi(\cdot)$ and $\Gamma(\cdot)$ are bounded uncertain functions, and, without loss of generality, the sign of the control gain χ is taken constant and strictly positive. Thus, there exist $K_m \in \mathbb{R}^{+*}$, $K_M \in \mathbb{R}^{+*}$, $C_0 \in \mathbb{R}^+$ such that

$$
0 < K_m < \Gamma < K_M \quad |\chi| \le C_0.
\tag{18}
$$

for $x \in \mathbf{X} \subset \mathbb{R}^n$, $\mathbf{X}$ being a bounded open subset of $\mathbb{R}^n$ within which the boundedness of the system dynamics is ensured.

The synthesis of a high order sliding mode controller for (16) is made through the following idea: switching variable is defined such that the system evolves, *early from $t = 0$*, on a switching manifold. Furthermore, the sliding variable and its time derivatives reach the origin in finite time in spite of uncertainties thanks to discontinuous control. The design of the controller consists in two steps

- design of the switching variable for (17),

- design of a discontinuous control input w maintaining the system trajectories on a switching manifold which ensures the establishment of a rth order sliding mode in finite time t_F, in spite of uncertainties.

The switching variable described in the sequel is an adaptation of the result of [33]. Of course, it ensures that *theorically*, a rth order sliding mode behavior is established in a *a priori* well-known time, and *practically* it ensures the stability of the system in a vicinity of the origin.

Switching variable. Let S the switching variable defined as

$$
S = s^{(r-1)}(x,t) - \mathcal{F}^{(r-1)}(t) + \lambda_{r-2}\left[s^{(r-2)}(x,t) - \mathcal{F}^{(r-2)}(t)\right] + \cdots + \lambda_0\left[s(x,t) - \mathcal{F}(t)\right]
\tag{19}
$$

with $\lambda_{r-2}, \cdots, \lambda_0$ such that $P(z) = z^{(r-1)} + \lambda_{r-2}z^{(r-2)} + \cdots + \lambda_0$ is a Hurwitz polynomial in the complex variable z. The function $\mathcal{F}(t)$ is a C^r-one defined as

$$
\begin{aligned}
s[x(0),0] &= \mathcal{F}(0), & s[x(t_F),t_F] &= \mathcal{F}(t_F) = 0, \\
\dot{s}[x(0),0] &= \dot{\mathcal{F}}(0), & \dot{s}[x(t_F),t_F] &= \dot{\mathcal{F}}(t_F) = 0, \\
&\vdots & &\vdots \\
s^{(r-1)}[x(0),0] &= \mathcal{F}^{(r-1)}(0), & s^{(r-1)}[x(t_F),t_F] &= \mathcal{F}^{(r-1)}(t_F) = 0
\end{aligned}
\tag{20}
$$

This choice ensures that the system is evolving *early from $t = 0$* on the manifold $S = 0$, and that it is evolving on $\mathcal{S}^r$ *from exactly $t = t_F$*. A solution for $\mathcal{F}(t)$ reads as ($1 \le j \le r$) [33]

$$
\mathcal{F}(t) = Ke^{Ft}Ts^{(r-j)}(0)
\tag{21}
$$

with F a $2r \times 2r$-dimensional stable matrix (strictly negative eigenvalues) and T a $2r \times 1$-dimensional vector.

H4. The integer j is such that $s^{(r-j)}(0) \ne 0$ and bounded.

---

[3]Given $a(x)$ a real-valued function and $b(x)$ a vector field, both defined on $\mathbf{X} \subset \mathbb{R}^n$, the derivative of $a(\cdot)$ along $b(\cdot)$ is written as $L_b a$ and is defined as $L_b a = \frac{\partial a}{\partial x}b(x)$ [18].

Lemma 1 ([33]) *There exist a stable matrix F and a matrix T such that $2r \times 2r$-dimensional matrix $\mathcal{K}$ defined as*

$$\mathcal{K} = \left[F^{r-1}Ts^{(r-j)}(0) \mid F^{r-1}e^{Ft_F}T \mid F^{r-2}Ts^{(r-j)}(0) \mid F^{r-2}e^{Ft_F}T \mid \cdots \mid Ts^{(r-j)}(0) \mid e^{Ft_F}T \right] \qquad (22)$$

is invertible.

From Lemma 1, as system (20) of $2r$ equations is linear in the $1 \times 2r$-dimensional gain matrix K, its resolution is then trivial and there exists always only a single solution

$$K = \left[s^{(r-1)}(0)\ 0\ s^{(r-2)}(0)\ 0\ \cdots\ s(0)\ 0 \right] \cdot \left[\mathcal{K}^T \right]^{-1} \qquad (23)$$

H5. There exists a finite positive constant $\Theta \in \mathbb{R}^+$ such that

$$\left| KF^r e^{Ft}Ts^{(r-j)}(0) - \lambda_{r-2}\left[s^{(r-1)} - KF^{r-1}e^{Ft}Ts^{(r-j)}(0) \right] - \cdots - \lambda_0\left[\dot{s}(x,t) - KFe^{Ft}Ts^{(r-j)}(0) \right] \right| < \Theta \qquad (24)$$

Equation $S = 0$ describes the desired dynamics which satisfy the finite time stabilization of vector $[s^{(r-1)}\ s^{(r-2)}\ \cdots\ s]^T$ to zero. Then, the *switching manifold* on which system (17) is forced to slide on via the discontinuous control w, is defined as

$$\mathcal{S} = \{x \mid S = 0\}. \qquad (25)$$

Given equation (20), one gets $S(t = 0) = 0$: at the initial time, the system still evolves on the switching manifold. There is no reaching phase in opposition to previous approaches as [21, 22].

Controller design. The attention is now focused on the design of the discontinuous control law w which forces the system trajectories of (17) to slide on $\mathcal{S}$, to reach in finite time the origin and to maintain the system at the origin.

Theorem 1 ([33]) *Consider the nonlinear system (16) with a relative degree r. Suppose that it is minimum phase and that hypotheses H1, H2, H3 and H4 are fulfilled. Let r be the sliding mode order and $0 < t_F < \infty$ the desired convergence time. Define $S \in \mathbb{R}$ by (19) with K unique solution of (21) given by (23) and suppose that assumption H5 is fulfilled. The control input w defined by*

$$w = -\alpha\,\mathrm{sign}(S) \qquad (26)$$

with

$$\alpha \geq \frac{C_0 + \Theta + \eta}{K_m}, \qquad (27)$$

C_0, K_m defined by (18), Θ defined by (24), $\eta > 0$, leads to

$$s = \dot{s} = \cdots = s^{(r-1)} = 0$$

at $t = t_F$. ∎

Sketch of proof. Condition (27) allows to satisfy the η-attractivity condition $\dot{S}S \leq -\eta|S|$. For more details, see [33].

In order to ensure the establishment of rth order sliding mode behaviour, and given that s and its $(r-1)$ first time derivatives equal 0 at $t = t_F$, control w is designed for $t > t_F$ only in order to maintain these latter equalities, which gives

$$w = -\alpha\,\mathrm{sign}(S)$$

$$S = \begin{cases} s^{(r-1)} - KF^{r-1}e^{Ft}Ts^{(r-j)}(0) + \lambda_{r-2}\left[s^{(r-2)} - KF^{r-2}e^{Ft}Ts^{(r-j)}(0) \right] \\ \quad + \cdots + \lambda_0\left[s - Ke^{Ft}Ts^{(r-j)}(0) \right] & \text{for } 0 \leq t \leq t_F \\[2mm] s^{(r-1)} + \lambda_{r-2}s^{(r-2)} + \cdots + \lambda_0 s & \text{for } t > t_F \end{cases} \qquad (28)$$

5.2 Application to pneumatic actuator position control

The objective consists in designing a robust (with respect to uncertainties/disturbances) position controller: then, define s the sliding variable as $s = y - y_d(t)$. From (5), its relative degree with respect to u_S equals 3, which implies that a 3rd order sliding mode controller can be designed. One has

$$s^{(3)} = \tilde{\chi}(\cdot) + \tilde{\Gamma}(\cdot)u_S \tag{29}$$

with

$$
\begin{aligned}
\tilde{\chi}(\cdot) &= (M^{-1} + \delta M)(1.2 + \Delta k)r_g(T + \Delta T)S\left(\frac{\varphi_P + \Delta\varphi}{V_P(y)} - \frac{\varphi_N + \Delta\varphi}{V_N(y)}\right) \\
&\quad - (M^{-1} + \delta M)(1.2 + \Delta k)S^2 v\left(\frac{p_P}{V_P(y)} - \frac{p_N}{V_N(y)}\right) \\
&\quad - (M^{-1} + \delta M)^2(b_v + \Delta b_v)\left(S(p_P - p_N) - (b_v + \Delta b_v)v\right) - y_d^{(3)} \\
\tilde{\Gamma}(\cdot) &= (M^{-1} + \delta M)(1.2 + \Delta k)r_g(T + \Delta T)S\left(\frac{\psi_P + \Delta\psi}{V_P(y)} + \frac{\psi_N + \Delta\psi}{V_N(y)}\right)
\end{aligned}
\tag{30}
$$

The control law is defined as[4] $u_S = \Gamma_{nom}^{-1} \cdot [-\chi_{nom} + w]$ with Γ_{nom} (resp. χ_{nom}) the nominal value of $\tilde{\Gamma}$ (resp. $\tilde{\chi}$), *i.e.* derived from (30) with no uncertainty. Note that Γ_{nom} is always strictly positive: then, u_S has the same sign as $(-\chi_{nom} + w)$. From (29), χ_{nom} and w are independent of u. One gets

$$s^{(3)} = \chi(\cdot) + \Gamma(\cdot)w \tag{31}$$

with $\chi = \tilde{\chi} - \tilde{\Gamma}\Gamma_{Nom}^{-1}\chi_{Nom}$ and $\Gamma = \tilde{\Gamma}\Gamma_{Nom}^{-1}$. As introduced in Section 5.1, the design follows two steps. The first one consists in computing off-line matrix K (equation (23)) which gives function $\mathcal{F}(t)$ (equation (21)). This latter and their time derivatives are computed on-line in order to ensure the convergence of s, $\dot{s}$, and $\ddot{s}$ to 0 at a fixed time t_F. The second step is the synthesis of discontinuous control which ensures the convergence in spite of uncertainties.

Switching variable. The switching variable S reads as (from (28))

$$
S = \begin{cases}
\dddot{s} - KF^2 e^{Ft}Ts(0) + 2\xi\omega_n\left[\dot{s} - KFe^{Ft}Ts(0)\right] + \omega_n^2\left[s - Ke^{Ft}Ts(0)\right] & \text{for } 0 \leq t \leq 0.5 \\
\dddot{s} + 2\xi\omega_n\dot{s} + \omega_n^2 s & \text{for } t > 0.5
\end{cases}
\tag{32}
$$

with $\xi = 1$, $\omega_n = 250 \ rad \cdot s^{-1}$ (ω_n has been chosen close to the open-loop proper frequency ω_{ol}). Initial conditions are $\ddot{s}(0) = 0 \ ms^{-2}$, $\dot{s}(0) = 0 \ ms^{-1}$ and $s(0) = 0.020 \ m$. The convergence time is stated as $t_F = 0.5 \ sec$. K is computed from (23) with F and T defined as (Lemma 1)

$$
T = \begin{bmatrix} 1 \\ 1 \\ 1 \\ 1 \\ 1 \\ 1 \end{bmatrix}, \qquad
F = \begin{bmatrix}
-1 & 0 & 0 & 0 & 0 & 0 \\
0 & -1.1 & 0 & 0 & 0 & 0 \\
0 & 0 & -1.2 & 0 & 0 & 0 \\
0 & 0 & 0 & -1.3 & 0 & 0 \\
0 & 0 & 0 & 0 & -1.4 & 0 \\
0 & 0 & 0 & 0 & 0 & -1.5
\end{bmatrix}
\tag{33}
$$

Discontinuous part w. $w = -\alpha \cdot \text{sign}(S)$ with $\alpha = 12 \cdot 10^4$ (in order to satisfy (27) by taking into account the bounded uncertainties and mass variations (+125%)).

Experimental results. As detailed in previous section, "Nominal case" and "Robust case"' tests are made, in order to evaluate performances and robustness of the controller.

---

[4]An interest of equivalent control is to reduce the value of discontinuous part gain [10] which implies a reduction of chattering effect.
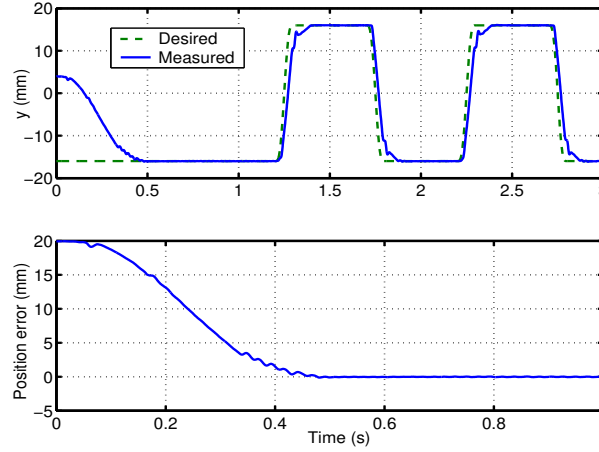
Figure 10: **Nominal case -Top.** Desired and current positions (*mm*) versus time (*s*). **Bottom.** Position tracking error (*mm*) versus time (*s*).
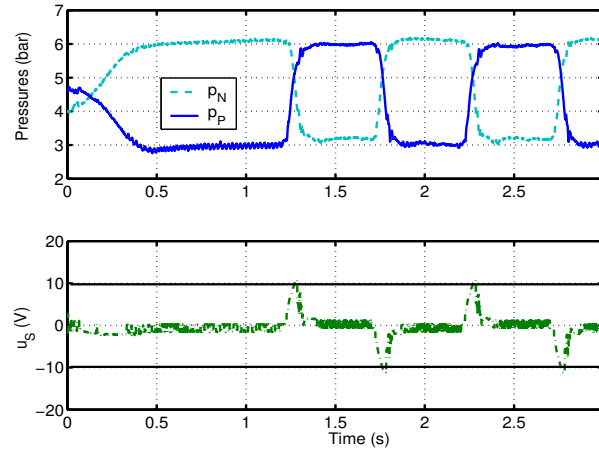

Figure 11: **Nominal case -Top.** Pressures p_P and p_N (*bar*) versus time (*s*). **Bottom.** Control signals u_P and u_N (*V*), and saturation line (*V*) versus time (*s*).

Nominal case. The actuator position (Figure 10) converges to the desired trajectory in 0.5*s* as scheduled *without control saturation* (Figure 11-Bottom). The maximum position error in steady state is 0.02*mm* in spite of springs forces. There is no pressure saturation (Figure 11-Top). In order to compare performances between gain scheduling and high order sliding mode SISO controllers, static position errors are summarized in Table 3. Recalling that the maximum position error allowed by the benchmark is 0.2 *mm*, the sliding mode SISO controller fulfills this constraint, which is not the case for the gain scheduling one.

Altitude	Low	Medium	High
Gain scheduling SISO controller	0.48	0.38	0.16
Higher order sliding mode SISO controller	0.02	0.01	0.08

Table 3. Static position error (*mm*) with gain scheduling (top) and sliding mode SISO (bottom) controllers.

Robustness evaluation. (Figure 12). The controller still ensures convergence in 0.5*s* without overshoot or control saturation. In steady state, the maximum position error equals 0.02*mm* which confirms the efficiency and robustness of this controller.
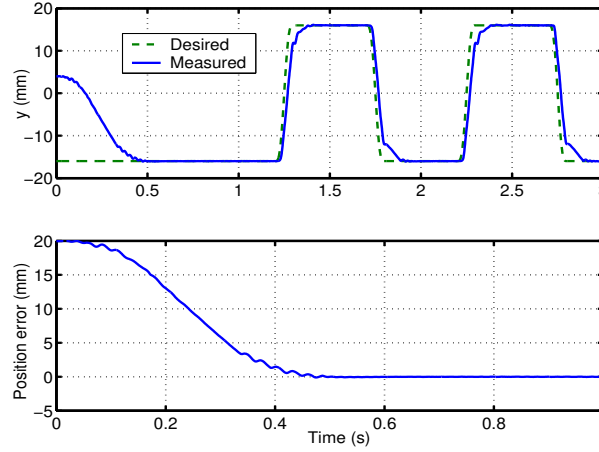
15

Figure 12: **Robustness Evaluation - Top.** Desired and current positions (*mm*) versus time (*s*). **Bottom.** Position tracking error (*mm*) versus time (*s*).
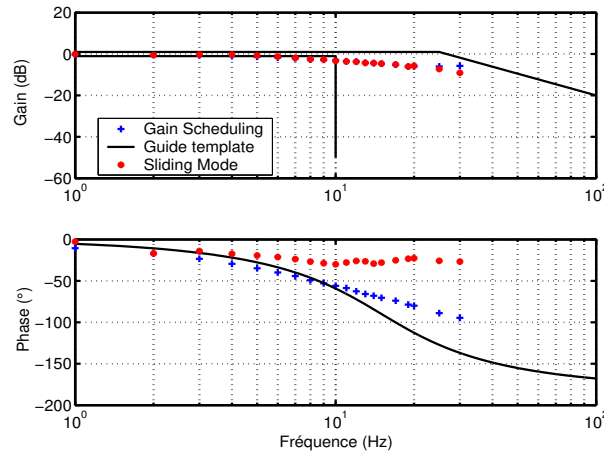

Figure 13: Closed-loop system Bode diagram.

Frequency response. (Figure 13) The frequency response is evaluated in the same conditions than previously. This test shows that, as previously mentioned in Section 4.2 (Frequency response item), the gain is not significantly improved by nonlinear control. However, the phase is now lower than the phase template which is not the case with linear controller and is a key-point with respect to desired performances.

Consumption. The consumption is evaluated by the same way than previously and results are displayed in Table 4. With the current controller, chattering effect appears and leads to high frequency control variations. These latter imply variation of mass flow rate during steady state position: the fluid consumption is increasing.

Controller	Gain scheduling SISO controller	Higher order sliding mode SISO controller
Consumption C_P	463 *g*	551 *g*
Consumption C_N	420 *g*	546 *g*

Table 4. Total consumption in each chamber during a flying sequence.

6 High order sliding mode position-pressure controller (MIMO)

Given the structure of the experimental setup, the use of two servodistributors allows to define two different control objectives. Then, in this section, a MIMO controller is displayed. As mentioned in Introduction, in order to improve system performances, in particular actuator positioning accuracy and rigidity, controller is now designed such both actuator position and pressure in one chamber are controlled. As pressure is now controlled, accuracy and rigidity are also improved, which is also a crucial point for steering mechanism application. Note also that, in MIMO case, there is no more zero dynamics, which ensures the stability of the whole system. The first objective consists in controlling actuator position, the second objective consisting in designing a robust pressure controller in order to fix pressure p_P in a high level (for rigidity and accuracy improvement). Define the sliding variables s_1 and s_2 as

$$s_1 = y - y_d(t) \qquad s_2 = p_P - p_{P_d}(t). \tag{34}$$

From (4), relative degree of s_1 w.r.t. u equals 3, which implies that *at least* a 3rd order sliding mode controller has to be designed for position. Relative degree of s_2 w.r.t. u equals 1 which implies that at least a 1st order sliding mode controller has to be designed for pressure. From (4), defining $h(x) = [h_1 \, h_2]^T := [y \, p_P]^T$, one gets

$$\begin{bmatrix} s_1^{(3)} \\ s_2^{(1)} \end{bmatrix} = \tilde{\chi}_M(x,t) + \tilde{\Gamma}_M(x) \cdot \begin{bmatrix} u_P \\ u_N \end{bmatrix} \tag{35}$$

with $\tilde{\chi}_M = \begin{bmatrix} L_f^3 h_1 - y_d^{(3)}(t) \\ L_f h_2 - \dot{p}_{P_d}(t) \end{bmatrix}$ and $\tilde{\Gamma}_M = \begin{bmatrix} L_{g_1} L_f^2 h_1 & L_{g_2} L_f^2 h_1 \\ L_{g_1} h_2 & 0 \end{bmatrix}$. Denoting $\tilde{\chi}_{M_{Nom}}$ and $\tilde{\Gamma}_{M_{Nom}}$ the nominal values (*i.e.* without uncertainty) of $\tilde{\chi}_M$ and $\tilde{\Gamma}_M$, the control input u reads as[5]

$$u = \begin{bmatrix} u_P \\ u_N \end{bmatrix} = \tilde{\Gamma}_{M_{Nom}}^{-1} \left[-\tilde{\chi}_{M_{Nom}} + \begin{bmatrix} \alpha_1 \cdot \text{sign}(S1) \\ \alpha_2 \cdot \text{sign}(S2) \end{bmatrix} \right] \tag{36}$$

with w the discontinuous input displayed in the sequel. From (35), one gets

$$\begin{aligned} \begin{bmatrix} s_1^{(3)} \\ s_2^{(1)} \end{bmatrix} &= \tilde{\chi}_M + \Gamma_M \left[\tilde{\Gamma}_{M_{Nom}}^{-1} \left[-\tilde{\chi}_{M_{Nom}} + w \right] \right] \\ &= \underbrace{\tilde{\chi}_M - \Gamma_M \tilde{\Gamma}_{M_{Nom}}^{-1} \tilde{\chi}_{M_{Nom}}}_{\chi} + \underbrace{\Gamma_M \tilde{\Gamma}_{M_{Nom}}^{-1}}_{\Gamma} w \end{aligned} \tag{37}$$

Switching vector S. The switching vector $S = [S_1 \, S_2]^T$ reads as (from (28))

$$\begin{cases} S_1 = \dddot{s}_1 - K_1 F_1^2 e^{F_1 t} T_1 s_1(0) + 2\xi_1 \omega_{n_1} \left[\dot{s}_1 K_1 F_1 e^{F_1 t} T_1 s_1(0) \right] + \omega_{n_1}^2 \left[s_1 - K_1 e^{F_1 t} T_1 s_1(0) \right] & \text{for } 0 \leq t \leq t_{F_1} \\ S_1 = \dddot{s}_1 + 2\xi_1 \omega_{n_1} \dot{s}_1 + \omega_{n_1}^2 s_1 & \text{for } t > t_{F_1} \end{cases}$$

$$\begin{cases} S_2 = s_2 - K_2 e^{F_2 t} T_2 s_2(0) & \text{for } 0 \leq t \leq t_{F_2} \\ S_2 = s_2 & \text{for } t > t_{F_2} \end{cases} \tag{38}$$

For S_1, one states $\xi_1 = 0.7$, $\omega_{n_1} = 180 \, rads^{-1}$, $t_{F_1} = 0.5 \, sec$, $\ddot{s}_1(0) = 0 \, ms^{-2}$, $\dot{s}_1(0) = 0 \, ms^{-1}$ and $s_1(0) = 0.020 \, m$. From (23), one gets

$$K_1 = \left[\ddot{s}_1(0) \, 0 \, \dot{s}_1(0) \, 0 \, s_1(0) \, 0 \right] \cdot \left[\left[\, F_1^2 T_1 s_1(0) \mid F_1^2 e^{F_1 t_{F_1}} T_1 \mid F_1 T_1 s(0) \mid F_1 e^{F_1 t_{F_1}} T_1 \mid T_1 s(0) \mid e^{F_1 t_{F_1}} T_1 \, \right]^T \right]^{-1}$$

---

[5]Matrix $\tilde{\Gamma}_M$ is invertible on the work domain

with F_1 and T_1 defined as (Lemma 1)

$$
T_1 = \begin{bmatrix} 1 \\ 1 \\ 1 \\ 1 \\ 1 \\ 1 \end{bmatrix} \qquad
F_1 = \begin{bmatrix}
-1 & 0 & 0 & 0 & 0 & 0 \\
0 & -1.1 & 0 & 0 & 0 & 0 \\
0 & 0 & -1.2 & 0 & 0 & 0 \\
0 & 0 & 0 & -1.3 & 0 & 0 \\
0 & 0 & 0 & 0 & -1.4 & 0 \\
0 & 0 & 0 & 0 & 0 & -1.5
\end{bmatrix}
$$

For S_2, one has $t_{F_2} = 0.5\ sec$, $s_2(0) = 5\ bar$. From (23), one gets

$$
K_2 \quad = \quad [s_2(0)\ \ 0] \cdot \left[\left[\ T_2 s_2(0)\ |\ e^{F_2 t_{F_2}} T_2\ \right]^T \right]^{-1}
$$

with F_2 and T_2 defined as (Lemma 1)

$$
T_2 = \begin{bmatrix} 1 \\ 1 \end{bmatrix} \qquad
F_2 = \begin{bmatrix} -1 & 0 \\ 0 & -1.1 \end{bmatrix}
$$

Discontinuous input w. The input w is tuned through gains α_1 and α_2 in order to satisfy (27) by taking into account the uncertainties and variations of mass (+125%): the experimental tests have been made with $\alpha_1 = 2 \cdot 10^5$ and $\alpha_2 = 8 \cdot 10^6$.

Nominal case. The actuator position (Figure 14) converges to the desired trajectory in $t_{F1} = 0.5s$ without control saturation. The maximum position error in steady state is $0.02mm$ in spite of springs force disturbance. There is no pressure saturation (Figure 15-Top). The control input is displayed in Figure 15-Bottom. In Table 5 are summarized results on static position error for different trajectories (corresponding to different altitudes flights). The MIMO high order sliding mode controller appears to be the most efficient controller w.r.t. the static position error.

Trajectory	Low	Medium	High
Gain scheduling SISO controller	0.48	0.38	0.16
Higher order sliding mode SISO controller	0.02	0.01	0.08
Higher order sliding mode MIMO controller	0.01	0.01	0.01

Table 5. Static position error (*mm*) with gain scheduling (Top), SISO sliding mode (middle) and MIMO sliding mode (bottom) controllers.

Robustness evaluation. (Figure 16). The controller ensures convergence in $0.5s$ without overshoot in spite of the mass variation. The maximum position error in steady state equals $0.02mm$ which confirms the efficiency/robustness of this controller.

Frequency response. (Figure 17). The frequency response is evaluated in the same conditions than previously, and the results are close to SISO ones.

Consumption. The desired pressure trajectory has been computed in order to have a maximum pressure in each chamber, which implies that rigidity is maximum with better accuracy. Experimental results also show that the high order sliding mode controller in MIMO case increases chattering on pressure p_P (as pressure controller is first order sliding mode one): it induces a more important consumption through the mass flow rate (see table 6). A solution would be to find, through an optimization way, a pressure trajectory with minimum consumption, maximum rigidity and/or to increase the order of sliding mode pressure controller.

Controller	Gain scheduling controller	Sliding mode SISO controller	Sliding mode MIMO controller
Consumption C_P	463 g	551 g	623 g
Consumption C_N	420 g	546 g	544 g

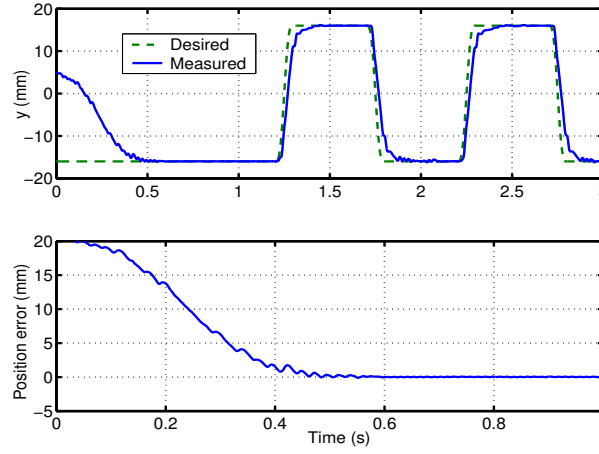Table 6. Total consumption in each chamber during a flying sequence.

Figure 14: **Nominal case - Top.** Desired and current positions (*mm*) versus time (*s*). **Bottom.** Position tracking error (*mm*) versus time (*s*).
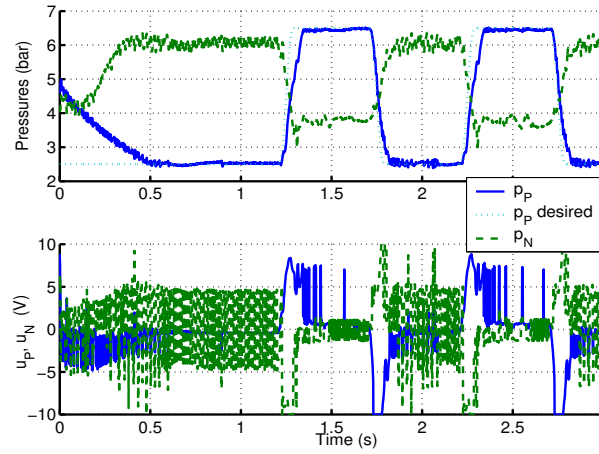

Figure 15: **Nominal case - Top.** Pressures p_P and p_N (*bar*) versus time (*s*). **Bottom.** Control signals u_P and u_N (*V*) versus time (*s*).
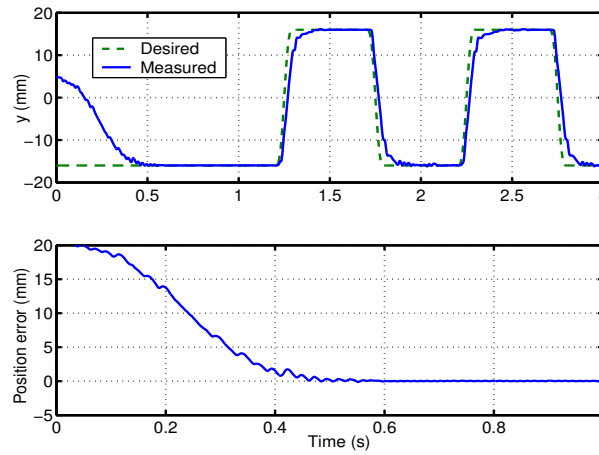

Figure 16: **Robustness evaluation - Top.** Desired and current positions (*mm*) versus time (*s*). **Bottom.** Position tracking error (*mm*) versus time (*s*).
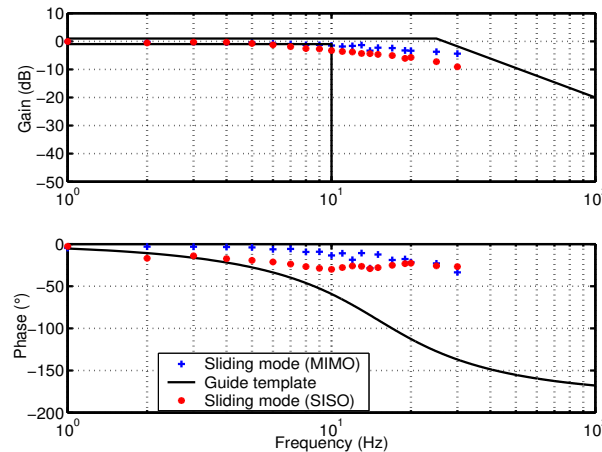
Figure 17: Bode diagram of closed-loop system.

7 Conclusion

The structure of the experimental setup and the benchmark (on which controllers are evaluated) are designed in order to check the use of such actuator in aeronautic context. In order to validate the benchmark performances, three controllers are designed. Experiments show that a linear gain scheduling feedback controller is not sufficient for this application. Higher order sliding mode controllers (SISO and MIMO) fulfill the main benchmark objectives. However, one of the performance criteria, the bandwidth at $-1\ dB$ of the closed-loop system, is still limited. In order to improve this point, a solution is the use of an other servodistributor able to ensure a higher mass flow rate. An other key point is the fluid consumption: high order sliding mode controllers need more fluid, but have greatly better accuracy and robustness performances. A future work will consist in designing pressure trajectory references (through optimization study) such that accuracy and robustness are kept.

Acknowledgment

References

[1] G. Bartolini, A. Ferrara, and E. Usai, "Chattering avoidance by second-order sliding mode contro", *IEEE Trans. Automat. Control*, vol.43, no.2, 1998, pp.241-246.

[2] M. Belgharbi, D. Thomasset, S. Scavarda, and S. Sesmat, "Analytical model of the flow stage of a pneumatic servo-distributor for simulation and nonlinear control", *in Scandinavian International Conference on Fluid Power SICFP'99*, Tampere, Finland, 1999, pp.847-860.

[3] M. Bouri, and D. Thomasset, "Sliding control of an electropneumatic actuator using an integral switching surface", *IEEE Trans. Control Syst. Technology*, vol.2, no.2, 2001, pp.368-375.

[4] X. Brun, S. Sesmat, D. Thomasset, and S. Scavarda, "A comparative study between two control laws of an electopneumatic actuator", *in European Control Conference ECC'99*, Karlsruhe, Germany, 1999.

[5] X. Brun, M. Belgharbi, S. Sesmat, D. Thomasset, and S. Scavarda, "Control of an electropneumatic actuator, comparison between some linear and nonlinear control laws", *Journal of Systems and Control Engineering*, vol.213, no.5, 1999, pp.387-406.

[6] X. Brun, D. Thomasset, S. Sesmat, and S. Scavarda, "Limited energy consumption in positioning control of electropneumatic actuator", *in Power Transmission and Motion Control*, Bath, UK, 1999, pp. 199-211.

[7] X. Brun, D. Morand , S. Scavarda, and D. Thomasset, "Contributions of the cosimulation in the chain of design of an electropneumatic system", *in International Conference on Fluid Power Transmission and Control ICFP 2001*, Hangzhou, China, 2001.

[8] M. Smaoui, X. Brun, and D. Thomasset, "A study on tracking position control of electropneumatic system using backstepping design", *Control Engineering Practice*, vol.14, no.8, 2006, pp.923-933.

[9] X. Brun, D. Thomasset, and E. Bideaux, "Influence of the process design on the control strategy: application in electropneumatic field", *Control Engineering Practice*, vol.10, no.7, 2002, pp.727-735.

[10] R. Castro-Linares, A. Glumineau, S. Laghrouche, and F. Plestan, "High order sliding mode observer-based control", *in 2nd IFAC Symposium on System, Structure and Control*, Oaxaca, Mexico, 2004.

[11] M.H. Chiang, C.C. Chen, and T.N. Tsou "Large stroke and high precision pneumaticpiezoelectric hybrid positioning control using adaptive discrete variable structure control", *Mechatronics*, vol.15, 2005, pp.523545.

[12] K.A. Edge, "The control of fluid power systems - responding to the challenge", *Journal of Systems and Control Engineering*, vol.211, no.2, 1997, pp.91-110.

[13] V. Fromion, and G. Scorletti, "A theoretical framework for gain scheduling", *International J. Robust and Nonlinear Control*, vol.13, no.10, pp.951-982, 2003.

[14] A.F. Filippov, *Differential Equations with Discontinuous Right-Hand Side*, Kluwer, Dordrecht, The Netherlands, 1988.

[15] A. Girin, F. Plestan, X. Brun, and A. Glumineau, "A third order sliding mode controller based on integral sliding mode for an electropneumatic system", *in IEEE Conference on Decision and Control CDC06*, San Diego, California, USA, 2006.

[16] K. Hamiti, A. Voda-Besançon, and H. Roux-Buisson, "Position control of a pneumatic actuator under the influence of stiction", *Control Engineering Practice*, vol.4, no.8, 1996, pp.1079-1088.

[17] G.F. Franklin, J.D. Powell, and A. Emani-Naeini, *Feedback Control of Dynamic Systems*, Addison-Wesley, Reading, Massachusetts, USA, 1987.

[18] A. Isidori, "Nonlinear control cystems: an introduction - Third edition", Spiringer-Verlag, Berlin, Germany, 1995.

[19] T. Kimura, S. Hara, T. Fujita, and T. Kagawa, "Feedback linearization for pneumatic actuator systems with static friction", *Control Engineering Practice*, vol.5, no.10, 1997, pp.1385-1394.

[20] A. Kyoungkwan, and Y. Shinichi, "Intelligent switching control of pneumatic actuator using on/off solenoid valves", *Mechatronics*, vol.15, 2005, pp.683-702.

[21] S. Laghrouche, F. Plestan, and A. Glumineau, "Practical higher order sliding mode control: optimal control based approach and application to electromechanical systems", Advances in Variable Structure and Sliding Mode Control, *Lecture Notes in Control and Information Sciences*, Springer-Verlag, Eds. Edwards C., Fossas Colet E., Fridman L., vol.334, 2006.

[22] S. Laghrouche, M. Smaoui, F. Plestan, and X. Brun, "Higher order sliding mode control based on optimal approach of an electropneumatic actuator", *International Journal of Control*, vol.79, no.2, 2006, pp.119-131.

[23] S. Laghrouche, F. Plestan, and A. Glumineau, "Higher order sliding mode control based on integral sliding mode", *Automatica*, vol.43, no.3, 2007, pp.531-537.

[24] D.J. Leith, and W.E. Leithead, "Survey of gain-scheduling analysis and design", *International Journal of Control*, vol.73, no.11, 2000, pp.1001-1025.

[25] A. Levant, "Sliding order and sliding accuracy in sliding mode control", *International Journal of Control*, vol.58, no.6, 1993, pp.1247-1263.

[26] A. Levant, "Universal SISO sliding-mode controllers with finite-time convergence", *IEEE Trans. Automat. Control*, vol. 46, no.9, 2001, pp.1447-1451.

[27] A. Levant, L. Alelishvili, "Integral high-order sliding modes", *IEEE Trans. Automat. Control*, vol.52, no.7, 2007, pp.1278-1282.

[28] A. Kellal, S. Scavarda, and J.G. Fontaine, "Electropneumatic servodrive for a robot", *in 16th Int. Symp. on Ind. Robots ISIR*, Brussels, Belgium.

[29] T. Miyajima, T. Fujita, K. Sakaki, K. Kawashima, and T. Kagawa, "Development of a digital control system for high-performance pneumatic servo valve", *Precision Engineering*, vol.31, 2007, pp.156-161.

[30] S. Ming-Chang, and T. Shy-I, "Identification and position control of a servo pneumatic cylinder", *Control Engineering Practice*, vol.3, no.9, 1995, pp.1285-1290.

[31] A.K. Paul, J.K. Mishra, and M.G. Radke, "Reduced order sliding mode control for pneumatic actuator", *IEEE Trans. Control Syst. Technology*, vol.2, no.3, 1994, pp.271-276.

[32] F. Plestan, S. Laghrouche, and A. Glumineau, "Multivariable practical higher order sliding mode control", *in IEEE Conference on Decision and Control - European Control Conference CDC-ECC'05*, Sevilla, Spain, 2005.

[33] F. Plestan, A. Glumineau, and S. Laghrouche, "A new algorithm for high-order sliding mode control", *International J. Robust and Nonlinear Control*, vol.18, no.4-5, pp. 441-453, 2008.

[34] R.T. Reichert, "Dynamic scheduling of modern-robust-control autopilot designs for missiles", *IEEE Control Systems Magazine*, vol.12, no.5, pp. 35-42, 1992.

[35] E. Richard, and S. Scavarda, "Comparison between linear and lonlinear control of an electropneumatic servodrive", *J. of Dynamic Systems, Measurement, and Control*, vol.118, 1996, pp.245-252.

[36] W.J. Rugh, and J.S. Shamma, "A survey of research on gain scheduling", *Automatica*, vol.36, no.10, 2000, pp.665-671.

[37] S. Sesmat, and S. Scavarda, "Static characteristics of a three way servovalve", *in Conference on Fluid Power Technology*, Aachen, Germany, 1996.

[38] J.L. Shearer, "Study of pneumatic processes in the continuous control of motion with compressed air", *Trans. Am. Soc. Mech. Eng.*, vol.78, 1956, pp.233-249.

[39] M. Smaoui, X. Brun, and D. Thomasset, "A robust differentiator-controller design for an electropneumatic system", *in IEEE Conference on Decision and Control - European Control Conference CDC-ECC'05*, Sevilla, Spain, 2005.

[40] Z. Rao, and G.M. Bone, "Modeling and Control of a Miniature Servo Pneumatic Actuator", *in IEEE International Conference on Robotics and Automation ICRA'06*, Orlando, Florida, USA, 2006.

[41] H. Schultea, and H. Hahn, "Fuzzy state feedback gain scheduling control of servo-pneumatic actuators", *Control Engineering Practice*, vol.12, no.5, 2004, pp.639650.

[42] M.Smaoui, X.Brun, and D. Thomasset, "A combined first and second order sliding mode approach for position and pressure control of an electropneumatic system", *in American Control Conference ACC'05*, Portland, Oregon, 2005.

[43] M. Smaoui, X. Brun, and D. Thomasset, "A study on tracking position control of electropneumatic system using backstepping design", *Control Engineering Practice*, vol.14, no.8, 2006, pp.923-933.

[44] M. Smaoui, X. Brun, and D. Thomasset, "Systematic control of an electropneumatic system: integrator backstepping and sliding mode control", *IEEE Trans. Control Syst. Technology*, vol.14, no.5, 2006, pp.905-913.

[45] L. Yang, and J.H. Lilly, "Sliding mode tracking for pneumatic muscle actuators in bicep/tricep pair configuration", *in American Control Conference ACC'03*, Denver, Colorado, 2003.